Energy Efficiency (2017) 10:405–417
DOI 10.1007/s12053-016-9461-8

ORIGINAL ARTICLE

Optimal and energy efficient operation of conveyor belt systems with downhill conveyors

Tebello Mathaba · Xiaohua Xia

Received: 8 June 2015 / Accepted: 27 June 2016 / Published online: 8 July 2016

Abstract Downhill conveyors are important potential energy sources within conveyor belt systems (CBSs). Their energy can be captured using regenerative drives. This paper presents a generic optimisation model for the energy management of CBSs that have downhill conveyors. The optimisation model is able to optimally schedule three configurations of a case-study CBS that is connected to the grid and operated under a time-of-use tariff. The three suggested drive configurations showcase potential energy savings/incomes that can be obtained from implementing: (a) variable speed control, (b) internal use of downhill conveyor energy and (c) the export of energy to the grid. The results show that a CBS with a daily energy consumption of 924 kWh can be reconfigured and controlled to reduce consumption by 53 or 100 % or be made to generate 1984 kWh, depending on the configuration. Analysis of the investment in each of the three configurations is assessed using a life-cycle cost and payback period (PBP). The daily operation simulation results show that the use of regenerative drives and variable speed control is able to provide energy savings in CBSs. The cost analysis shows that the configuration that enables sale of energy to the grid is the most profitable arrangement, for the case study plant under consideration. The sensitivity analysis indicates that the PBPs are more sensitive to the annual electricity price increases than changes in the discount rate. Combining regenerative drives and optimal operation of CBS generates energy savings that give attractive PBPs of less than 5 years.

Keywords Energy management · Energy efficiency · Conveyor belt · Regenerative drives · Demand response

T. Mathaba (✉)
EECE Department, University of Pretoria, Pretoria 0002, South Africa
e-mail: tmathaba@tuks.co.za

Introduction

Conveyor belt systems (CBSs) are used in a variety of industries for bulk material transportation, as outlined by Fedorko et al. (2014). It is a well-known fact that energy consumption of conveyor belt systems (CBSs) is lowered by implementing variable speed drives (VSDs) instead of fixed speed drives (Zhang and Xia 2010; Ristić and Jeftenić 2012; Hiltermann et al. 2011; Middelberg et al. 2009; Saidur et al. 2012; de Almeida et al. 2005). CBSs are typically made up of storage units and a series of belt conveyors, some of which maybe downhill. Downhill conveyors (DHCs) tend to require a constant braking force in order to maintain a required operating speed. In addition to the required mechanical safety brakes, an electrical braking system is used (Rodríguez et al. 2002; Lűchinger et al. 2006; ABB 2011a). In general, the braking process is undesirable because it wastes energy, presents

a fire risk and reduces the motor's lifespan. An efficient alternative is to capture the braking energy and convert it into useful electrical energy (González-Gil et al. 2013; ABB 2011a).

Apart from VSDs, further attempts to achieve energy efficiency are leading to the introduction of regenerative drives (RDs) on downhill belts. DHCs have long been seen as potential sources of energy (Rodríguez et al. 2002; Lűchinger et al. 2006). The use of a 20-MW thyristor-based active front end (AFE) drive system to harness the power of DHCs in an iron-ore mine is reported in Rodríguez et al. (2002). Lűchinger et al. (2006) also reports on the application of an insulated-gate bipolar transistor (IGBT)-based AFE drive on conveyors of a cement plant to potentially generate over 700 kW of power. The application of RD technology is increasingly gaining interest in the power and energy research community. Its other application areas include passenger transportation and overhead cranes (González-Gil et al. 2013; Zhang et al. 2013; Musolino et al. 2011; Mitrovic et al. 2012). The current research on the application of RDs tends to focus on power quality-related issues, and not enough attention has been given to energy management and cost issues (Rodríguez et al. 2002; Lűchinger et al. 2006; Mitrovic et al. 2012). The latter two issues are the key focus of this paper.

Changes in tariffs towards more sophisticated electricity pricing schemes is one of the dominant trends in the electricity markets. This trend is motivated by the increasing need for utilities to influence demand and offer the most equitable prices for electricity (Mathaba et al. 2014). Some of the progressive tariffs, such as Eskom's[1] newly proposed Genflex allows consumers to sell power back to the grid (Eskom 2013b). Tariffs such as this make energy efficiency interventions capable of producing power even more attractive. Thus, VSDs and RDs can be used in combination with optimal scheduling to deliver more cost benefit from CBSs under price-responsive demand response programmes such as those outlined by Pelzer et al. (2008), and Gellings and Samotyj (2013).

Predictably, the decision to install VSDs/RDs is motivated by their economic viability within a particular plant, and this depends on the amount of potential energy savings or incomes. It is therefore necessary to accurately model and predict the amount of savings/incomes to be made from the energy saved/generated by investing in VSDs and RDs.

This paper presents an optimal scheduling model and three drive configuration options that can be used to improve the energy efficiency of CBSs with DHCs. The proposed generic optimisation model can calculate optimal schedules for the three different configurations of drives while taking into consideration the CBS's operational constraints. Besides improving energy efficiency, the model also minimises the electricity cost by taking advantage of the electricity tariff. The economic benefit of implementing VSDs and RDs on CBS with DHCs is analysed for a case study plant. The proposed model quantifies the potential amount of energy savings or incomes and can be used to help a CBS operator decide on the economic viability of investing in appropriate drive technology. The analysis in this paper is novel because the newly proposed optimisation model facilitates energy management of CBSs that are able to sell electricity to the grid.

Background

Conveyor drive technology

For variable speed control (VSC), a conveyor alternating current (AC) motor is driven by a VSD fed by a three-phase supply. AC motor VSDs come in a wide variety of configurations, inverter topologies and control techniques. The more common topologies are the direct converters such as Cyclo-converters, and indirect converters like the current source inverters and voltage source inverters (VSIs). The VSIs are further sub-classified into two-level or multi-level depending on the number of voltage levels generated. A thorough analysis of the classification is beyond the scope of this paper, and it can be found in (Bose 2002; Rodríguez et al. 2002; Kouro et al. 2012). The different types of commonly applied control techniques are scalar control, vector or field-oriented control, direct torque control (DTC) and intelligent control (Bose 2002; ABB 2011b). Above all these, a VSD can either be regenerative or non-regenerative.

Figure 1 shows the high-level components of a typical DTC non-regenerative VSI VSD, with dynamic braking. The diode/IGBT rectifier converts the incoming AC to direct current (DC). The DC link has a capacitor bank that filters the DC from the rectifier.

[1] www.eskom.co.za (a South African state-owned utility)

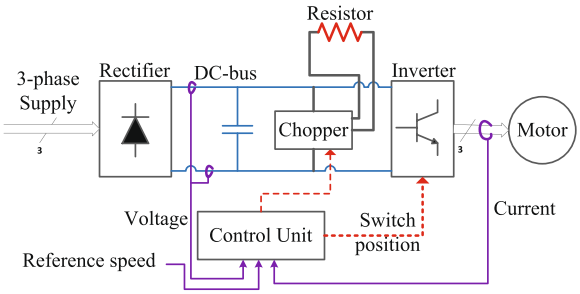

Fig. 1 Components of a non-regenerative variable speed drive (A DTC drive of a VSI topology with dynamic braking)

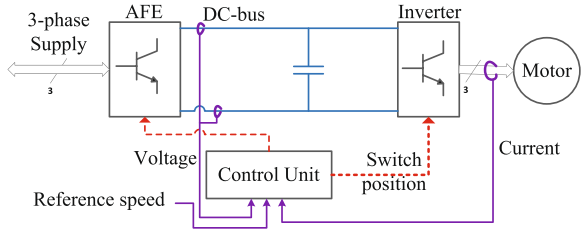

Fig. 2 Components of a regenerative variable speed drive

Based on a control signal, the inverter then converts the filtered DC back to an AC, the frequency of which is dictated by the control unit's switch positions. The AC motor is energised by the inverter to rotate at the speed proportional to the output AC frequency. (ABB 2011a; Mitrovic et al. 2012; Saidur et al. 2012; de Almeida et al. 2005).

The DTC technique uses an in-build mathematical motor model, as well as feedback signals of the DC-bus voltage and line currents, to calculate the values of the motor's torque and flux. The DTC control unit then uses the calculated torque and flux information to generate the inverters' switch positions that will turn the motor at the speed equal to the input reference speed (Bose 2002).

The load on a DHC produces a torque that rotates the motor's shaft to generate electrical energy. This energy is transmitted back into the drive to charge the DC-link's capacitor. This results in a raised DC-bus voltage because the energy cannot flow out through the rectifier. To avoid equipment failure, the DC voltage has to be restored to its normal level. A dynamic braking unit (BU) connected to the VSD achieves braking by absorbing the energy on the DC-bus and hence lowering the DC voltage. Figure 1 show the BU made up of a chopper and a power resistor. The chopper is an electronic switch that connects a resistor to the DC-bus in order to dissipate the energy into heat whenever the DC voltage increases beyond the required level. During braking, the resistor becomes hot, and so an investment into a well-functioning ventilation system is sometimes needed to reduce the heat (ABB 2011a; Mitrovic et al. 2012).

Another alternative to wasting the braking energy of a DHC is capturing it using a regenerative VSD like the one illustrated in Fig. 2. Active front end (AFE) is one of the prominent regenerative drive technologies (Rodríguez et al. 2002; Lűchinger et al. 2006). In the AFE configuration, the VSD's input diode rectifier is replaced by a bi-directional transistor-based voltage source rectifier capable of directing power from the conveyor motor into the grid as detailed by Mitrovic et al. (2012). The energy generated from a DHC can either be used by other motors within the plant or sold to the grid. Not all power from the bulk material load is converted into electrical energy due to friction in the motor and mechanical subsystems attached to the shaft. A utility may also impose a transmission charge when the conveyor feeds power into the grid. The implementation of this technology is commonly packaged in AFE units that also include line filter and choke modules to improve the quality of power (Mitrovic et al. 2012; Schneider-Electric 2013).

The diode rectifier of the non-regenerative VSD makes it small, cheap and reliable when compared to the regenerative drive with more active devices in the AFE. However, the regenerative drive produces less low-order harmonics and is more energy efficient than the non-regenerative drive (Kouro et al. 2012).

In practice, multiple options for configuring AFE and inverter units are available to application engineers. For instance, a single inverter unit can be used to drive multiple motors. A common DC-bus can also be used to connect DC-links of multiple inverter units so that a regenerating motor simply injects energy into the DC-bus where other motors can use it, to reduce the load on the grid. The use of RD and choice of configuration needs to be justified by operational constraints and the amount of energy to be generated for a given plant layout (ABB 2011a; Mitrovic et al. 2012). These considerations shall be made so that investment into RDs/non-regenerative VSDs is economically viable for a conveyor belt operator. As a result, the ability to model the energy output of DHCs is crucial.

Conveyor belt energy model

A CBS operating schedule dictates the belt speed profile, $v(t)$ in m/s, together with corresponding feed-rate, $I(t)$ in kg/s. In practice, a typical CB schedule holds $v(t)$ and $I(t)$ constant for short durations of time, called sampling time $\triangle t$. This make the schedule's implementation easier (Mathaba et al. 2014; 2012). The amount of material on the belt is commonly specified in mass per unit length. Thus, $q(x,t)$ in kg/m is the mass per length of material at a given point, x, along the conveyor belt's length at a time, t. Conveyor belts are designed to carry material with little amounts of trampling from the tail to the head end. When $v(t) = v$ is constant, material flows along the conveyor belt like a constant speed wave (vanDelft 2010). Thus, according to Strauss (2008), the one-dimensional transport equation in (1) describes the flow of material on the belt.

$$\frac{\partial}{\partial t}q(x,t) = -v\frac{\partial}{\partial x}q(x,t). \tag{1}$$

For computing purposes, (1) can be discretised in a variety of ways (Strauss 2008). One of the stable finite difference methods for computing (1) is explained in the Appendix section. The mechanical energy driving a conveyor belt counters the total resistance of the belt F_U (ISO 1989). Equation 2 shows that F_U is made-up of primary resistance F_H, secondary resistance F_N, special resistance F_S and resistance due to the slope F_{St} (Zhang and Xia 2011). Primary resistance is the resistance due to flexing of the belt and material, as well as the rolling friction of the idlers. Secondary resistance is due to, the inertia and friction of the material as it lands on the belt, the wrap resistance between the belt and the pulley, and the resistance of the pulley bearings. Special resistance is due to special fitting on the conveyor such as tilted idlers, frictions of the skirt boards on the loading point and the belt ploughs at the discharge end. F_{St} is the resistance from the overall lowering or elevation of material. It is due to the height difference between the conveyor's loading and discharge points (ISO 1989).

$$F_U = F_H + F_N + F_S + F_{\mathrm{St}}. \tag{2}$$

Equation 2 can be further simplified to Eq. 3 by looking at general conditions of F_S and F_H in many conveyor installations. Special resistance occurs at the belt fitting on the head or tail of the belt and it is usually comparatively small, i.e $F_S \approxeq 0$ (Hiltermann et al. 2011). Secondary resistance can be written as a fraction of F_H, i.e. $F_N = F_H(C_M - 1)$, where $C_M \geq 1$. C_M decreases with increasing conveyor belt length, for example a 1.8 for a 100-m-long belt while it is 1.1 for 1-km-long belt (ISO 1989).

$$F_U \approxeq C_M F_H + F_{\mathrm{St}}. \tag{3}$$

The dominant primary resistance, $F_H = C_1 + C_2 \cdot \bar{q}$, has parameters, C_1 and C_2, whose values depend on the average load of the belt, $\bar{q} = \int_0^L q(x,t) \cdot dx$, the length of the belt L and an artificial coefficient of friction f . F_{St} depends on the height difference between the tail and head of the belt, H, and the acceleration due to gravity, g; therefore, $F_{\mathrm{St}} = gH \cdot \bar{q}$ (ISO 1989; CEMA 2005). Therefore, the electric power required to run the conveyor is given by,

$$P = \frac{1}{\eta}F_U \cdot v = \frac{1}{\eta}(\varphi_1 + \varphi_2\bar{q}) \cdot v, \tag{4}$$

where $\varphi_i, i \in [1,2]$ are the modelling parameters and η is the overall motor drive efficiency. The power model parameter values are given by,

$$\varphi_1 = C_M \cdot C_1 \text{ and} \varphi_2 = C_M \cdot C_2 + g \cdot H. \tag{5}$$

For DHCs, H is considered negative; thus, $gH < 0$. For belts with sufficiently steep profiles, the force of gravity on the bulk material dominates φ_2, and so $|C_M \cdot C_2(f)| < |gH|$. In such cases, the belt is capable of rolling downhill and turning the motor without any input power. This occurs whenever the mass of the material on the belt exceeds a critical value, $M_{\mathrm{crit}} = L \cdot \varphi_1 / |\varphi_2|$, and the conveyor is said to be operating in a regenerative mode.

Energy and cost optimisation

Case study plant

For a case study, they consider a CBS designed to transport limestone and clay from a mining area stockpile to a cement making facility similar to that in (Lűchinger et al. 2006), located in the Waterberg region of South Africa. Figure 3 shows a layout of the plant where CBS is run at a fixed speed. In many countries, the cement making industry accounts for a significant portion of national energy consumption. Raw material processing consumes about 28 % of electricity; therefore, DSM is important in this industry (Madlool et al. 2013). Due to the rugged terrain, a

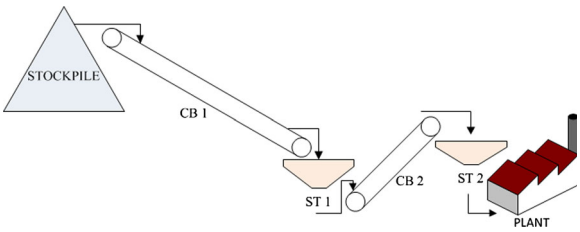

Fig. 3 Conveyor in a cement making plant

long conveyor system is used. The system operates at a maximum speed of 3.1 m/s to transport bulk material to a plant 280 m below the crushing station. In our model, we consider the 2.4-km-long DHC that receives quarry from the crusher and feeds it to a 600-m-long inclined conveyor that delivers material to a storage in a cement plant as shown in Fig. 3.

The considered CBS is set to feed an annual production capacity of 1,400,000 t which requires about 280 t/h of raw material. The system shown in Fig. 3 has a normal maximum throughput of 850 t/h while the plant silos, ST2, have a 6-h buffer storage of 1680 tons. The energy model parameter values (φ_1, φ_2) are (25.0 kN, -1.58×10^3 m^2/s^2) for CB1 and (9.78 kN, 105 m^2/s^2) for CB2. CB1 is capable of generating 296 kW, and CB2 can consume 55 kW of power at their maximum speed of 3.1 m/s and throughput of 850 t/h. The intermediate bulk storage ST1 is typically negligible in size, and it is located at a transfer station to facilitate the exchange of material between two belts.

Electricity pricing

Electricity supply constraints in countries such as South Africa are increasing the popularity of demand response programmes (Gellings and Samotyj 2013). The operation of the plant in Fig. 3 is considered under a time-of-use (TOU) tariff offered by Eskom's demand-side management programs. Mining operations are normally based in the rural areas; thus, the tariff called Ruraflex, given by Eq. 6, is appropriate to use for estimating the cost of energy consumption (Eskom 2013b).

$$\pi_n = \begin{cases} 0.40 \text{ R/kwh, off-peak } n \in [1-6, 23, 24] \\ 2.41 \text{ R/kwh, peak } n \in [7, 11-18, 21, 22] \\ 0.73 \text{ R/kwh, standard } n \in [8-10, 19, 20] \end{cases}. \tag{6}$$

The proposed Genflex tariff is used for calculating the income made from generating energy as well as cost of consumption. Under the Genflex tariff, independent power producers (IPPs) are able to use the utility's network to wheel their energy to a third party. The utility charges the IPP a use-of-system (UoS) charge for the use of its network. The IPP is able to get revenue for energy sales to a third party according to their power purchase agreement (PPA) (Eskom 2013a). The selling price of the IPP's energy has to be less than that of the utility by some factor Sf_n, in order to make it attractive to the third party.

The energy from the IPP is also subject to a flat-rate reliability charge π_{RC} and a time-dependent system loss charge. The reliability charge compensates the utility for providing good quality power and security of supply. The loss-charge accounts for the inevitable transmission losses incurred by the utility as it transmits the IPPs energy to loads connected to the utility. In Eskoms case, the utility simply assigns a loss-factor Lf_n based on the distance between the IPP's generator location and the location of utility's major load. This effectively reduces the IPP's output from a monetary perspective. Considering the selling price, reliability and loss charges, the TOU energy cost (EC) for an IPP are,

$$\mathrm{EC}_n = \begin{cases} \pi_n \cdot P_n^d \cdot \triangle t, & \text{when } P_n^d \geq 0 \\ (\pi_n \cdot \mathrm{Sf}_n \cdot \mathrm{Lf}_n - \pi_{\mathrm{RC}}) \cdot P_n^d \cdot \triangle t, & \text{when } P_n^d < 0, \end{cases} \tag{7}$$

where P_n^d is the magnitude of average power produced or consumed by the IPP during a time period n. Negative and positive values of P_n^d correspond to the generation and use of power, respectively. In addition to the energy cost (7) , the UoS charges are billed depending on whether the IPP is connected to the distribution or transmission network. Firstly, a standard administration and service charge π_{AS} is billed monthly per point-of-delivery and account. Secondly, the IPP incurs a network access charge π_{NA} based on the maximum power exported to the grid (or maximum demand required by the IPP) within a billing period. Thus, the monthly network access cost (NAC),

$$\mathrm{NAC}(P_n^d) = \max\left\{-P_n^d, P_n^d\right\} \cdot \pi_{NA} \tag{8}$$

For the purpose of our analysis, the following pricing values are used: π_{AS} = R512.10/month, π_{NA} = 9.40/kW, π_{RC}=0.20/kWh. π_{AS} represents the administration and service charge billed per month for account

Table 1 Summary of configuration options

Option	Equipment/component available			
	VSDs	BU on CB1	Common DC-bus	AFE
A	Yes	Yes	No	No
B	Yes	Yes	Yes	No
C	Yes	No	Yes	Yes

services rendered by the utility on each working day of the month. That is, days excluding weekends. The CB plant is assumed to sell its energy at a 10 % discount to the utility's TOU price, so $\mathrm{Sf}_n = 0.9$. The Lf_n associated with peak, standard and off-peak times are calculated to be 0.85, 0.85 and 0.75, respectively (Eskom 2013b).

Drive configuration options

In the following sections, we compare the optimal scheduling of the CB system under the three different configuration options with the base case design. In the base case design, the downhill CB1 is fitted with a 315-kW VSD and a braking unit, while both conveyors are operated at a constant maximum speed to meet the hourly material demand of 280 t/h. Electricity cannot be sold to the grid under the base case. Material demand when operating at full speed is 280 t/h. Under these conditions, CB1 consumed $P_n^1 = -45.4$ kW[2] while CB2 consumes $P_n^2 = 38.5$ kW. Thus, CB1 generates 1090 kWh and CB2 consumes 924 kWh of energy per day. From the utility's perspective, the plant's load profile is flat with an hourly consumption of 38.5 kW. Therefore, the plant's daily electricity cost under the tariff in Eq. 6 is R895.62.

The three different alternative configuration options and their implications on the energy and network access costs are subsequently explained. Unlike the base case, all the following options operate with variable speed control (VSC) to enable load-shifting. All options have a 315-kW VSD connected to CB1 and a smaller 75-kW VSD connected to CB2. The equipment used in each option is summarised in Table 1. The detailed descriptions of the options are as follows:

- Option A (VSC): The 315-kW VSD is connected to a braking unit connected, and the two VSDs are isolated . Option A is similar to the base case, because no electricity is sold to the grid. The only exception is the additional 75-kW VSD on CB2. The electricity is continually being consumed by CB2, even when CB1 produces more than the consumption of CB2. The only advantage over the base case is that this configuration is optimally operated using a variable speed. The energy cost, defined by Eq. 7, is modified to $\mathrm{EC}_n = \pi_n \cdot P_n^d \cdot \triangle t$, where P_n^d refers to the power consumed by CB2 only (i.e. $P_n^d = P_n^1$).
- Option B (VSC and internal use of energy): Each of the conveyors is connected to a VSD, and both VSDs are in turn connected by a common DC-bus, as shown in Fig. 4. This configuration is similar to that of option A, with the difference being the addition of the DC-bus. Option B is suitable when the individual conveyor belt drives are located in close proximity. Therefore, according to the layout in Fig. 3, the conveyor motors have to be located at the tail-end for CB1 and the head for CB2. The energy generated by CB1 can be used by CB2. Therefore, grid electricity is

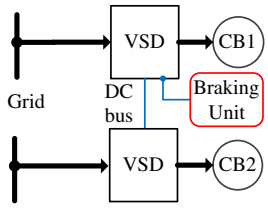

Fig. 4 Option **b** drive configuration

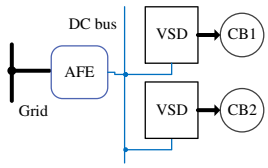

Fig. 5 Option **c** drive configuration

[2]Negative consumption implies generation.

used only when the consumption of CB2 exceed the generation of CB1 (i.e. $EC_n = 0$ whenever $P_n^d = P_n^1 + P_n^2 < 0$). So, (8) changes to $NAC = \pi_{NA} \cdot \max\{P_n^d\}$, and Eq. 7 is modified to $EC_n = \max\{0, \pi_n \cdot P_n^d \cdot \triangle t\}$.

– Option C (VSC and energy export): Each of the VSD driving the conveyors is connected to the grid through an AFE as shown in Fig. 5. Option C is also suitable for the conveyor drives that are located in close proximity to each other and when they are both close to a transformer. This reduces the length of connecting cables and hence the project costs. The braking unit is eliminated in this configuration because the AFE allows bi-directional transfer of power. When CB2 consumes more than what CB1 is producing, power P_n^d is purchased at a price π_n. Alternatively, when CB1 produces more power than the consumption of CB2, P_n^d becomes negative and the power is sold to a third party via the grid. Thus, the energy and networkaccess costs are as defined by Eqs. 7 and 8, respectively.

Optimal scheduling

For variable notation purposes, the superscript 1 denotes variables associated with the DHC and intermediate storage, while 2 is for those associated with CB2 and ST2. The optimal schedule manipulates speed v_n and feed rates I_n for each sampling time, n, to reduce the energy cost. A generic daily cost function of operating the plant shown in Fig. 3 , incorporating all UoS charges, energy incomes and belt mechanical costs is given by,

$$\begin{aligned}\mathrm{OpCost}(v_n^j, I_n^j) \;=\; & \sum_{n=1}^{N_t} \mathrm{EC}_n(P_n^d) + \pi_{AS} \cdot \frac{1}{20} \\ & + \mathrm{NAC}(P_n^d) \cdot \frac{1}{20} \\ & + \omega \sum_{n=1}^{N_t - 1} \sum_{j=1}^{2} (v_n^j - v_{n+1}^j)^2, \end{aligned} \tag{9}$$

where $P_n^d = P_n^1(\bar{q}_n^1, v_n^1) + P_n^2(\bar{q}_n^2, v_n^2)\ \forall n \in [0, N_t]$ is the power produced by the conveyor system, v_n^j, I_n^j & $\bar{q}_n^j\ \forall j \in \{1, 2\}$ are the belt speed, feed-rates and average material mass per belt, respectively. The value $\bar{q}_n^j = \frac{1}{N_{xj}} \sum_{i=1}^{N_x} q^j(i, n), \forall j \in \{1, 2\}$ is an average of linear densities sampled on N_{xj} equally spaced locations on each belt. The administration and service charge (π_{AS}) as well as NAC are spread over each of the monthly week days. The forth addend of Eq. 9 represents the mechanical cost. The mechanical cost ensures that the changes in belt speed are moderate to avoid excessive mechanical stress on the equipment. This is linked to the maintenance costs, and it has a direct link to the wear and tear of the belt, idlers and bearings. The significance of the addend relative to the energy cost is adjustable by acareful selection of ω, and it will depend on the conveyor operator's choice.

The optimal operating schedule $\{v_n, I_n\}^*$ has to meet the following operating constraints:

$$\Omega_1 : \left\{ \begin{array}{l} \widehat{A}_n^j \mathbf{q}_{n+1}^j = \mathbf{q}_n^j + \bar{\mathbf{b}}_n^j \cdot (I_n^j / 3.6 v_n^j), \\ v_{\min}^j \le v_n^j \le v_{\max}^j, I_{\min}^j \le I_n^j \le I_{\max}^j \\ q(0, n) \le Q_{\max}, \\ ST_L^1 \le ST_{n-1}^1 + v_n^1 \cdot q^1(N_{x1}, n-1) - \frac{\triangle t}{3.6} \cdot I_n^1 \le ST_U^1, \\ ST_L^2 \le ST_{n-1}^2 + v_n^2 \cdot q^2(N_{x2}, n-1) - \frac{\triangle t}{3600} \cdot D_n \le ST_U^2, \end{array} \right\}, \tag{10}$$

$\forall n \in [0, N_t]$ and $\forall j \in \{1, 2\}$. The first row of Eq. 10 is a discretisation of Eq. 1 that caters for material flow. Explanation of the discretisation technique, the matrix $\widehat{A}_n^j$ and vector $\bar{\mathbf{b}}_n^j$ is given in the Appendix. This row relates the vector of mass per unit lengths, $\mathbf{q}_n^j$, between time instances n and $n + 1$ using the parameters $\widehat{A}_n^j$ and $\bar{\mathbf{b}}_n^j$. The second and third rows of Eq. 10 define the actuator limits and belt carrying capacity, respectively. The last two rows of Eq. 10 ensure that storage limits are not exceeded. D_n represent the demand of bulk material and $\triangle t$ is the sampling time in the discrete domain. Therefore, the optimal operating schedule for

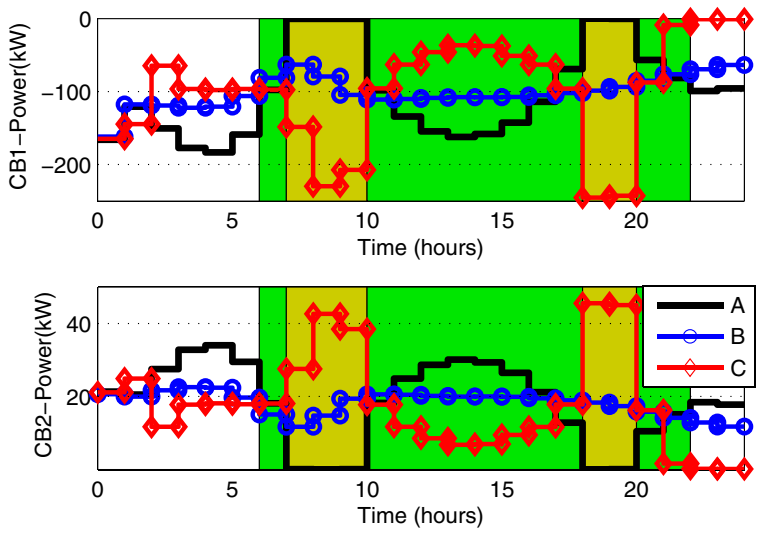

Fig. 6 Power consumption of each belt for the three options

the CB plant in Fig. 3 is the solution to the following optimisation problem,

$$\begin{aligned}
&\mathbf{min}_{\{v_n, I_n\}} \mathrm{OpCost}(v_n^j, I_n^j)\\
&\mathbf{s.t}\\
&\{v_n^j, I_n^j\} \in \Omega_1\\
&\Omega_2 : \{\textstyle\sum_{n=1}^{Nt} v_n^2 \cdot q^2(N_{x2}, n-1) = \sum_{n=1}^{Nt} \frac{\triangle t}{3600} \cdot D_n\}\\
&\text{given} \mathbf{q}_0^j \text{ and} ST_0^j,
\end{aligned} \tag{11}$$

where $\mathbf{q}_0^j$ and ST_0^j are the initial material distribution on the belt and amounts of material in storages. Each of the simulations begins with a storage at its minimum level. For the purpose of a fair analysis, an extra constraint, Ω_2, requiring that the storage level return to the minimum level at the end of the day, is imposed. The operation of the belt is optimal when its filled to capacity, i.e. $q(i,n) = Q_{\max}$. In order to get a fair analysis of the daily operations, the effect of the transients has to be eliminated. Therefore, $q^j(i,n) = \bar{q}$ and so $\bar{q} = Q_{\max}$. These modification eliminate the need for equality constraints in Eq. 10 and makes the problem easier to solve.

Figures 6 and 7 show the power and storage profiles for the three options. The different background shades in Figs. 6 and 7 correspond to the different periods of the TOU tariff prices given by Eq. 6. Figure 6 shows that unlike option B, option A's scheduling of CB2 avoids the peak times when electricity is most expensive. This is because all of CB1's energy is lost in option A and the utility always charges the plant for the consumption of CB2. However, option B uses the power generated by CB1 to power CB2. In contrast to both A and B, the scheduling under option C is shown to allocate most activity around peak times when the CBS can sell most of its energy at the maximum price. The storage profile on Fig. 7 shows that the capacity of ST2 restricts option A and C from avoiding and using peak times fully, respectively. However, option B does not fully use the storage capacity as it attempts maintain a balance of using CB2 to consume as much

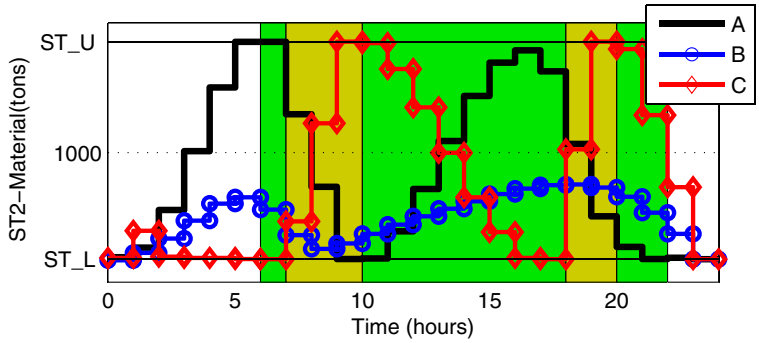

Fig. 7 Storage profiles of ST2 for the three options

energy as CB1 produces. This is sensible because under option B, all of the excess energy is wasted by dynamic braking.

In general, the optimised process of moving the daily load of material generates a total of 1984 kWh of energy. That is, CB1 generates 2422 kWh of energy while CB2 consumes 437 kWh. The optimised operation is more energy efficient than the full-speed operation of the base case where CB2 consumes 924 kWh per day. As a result, the optimal scheduling of the plant saves energy under each of the three options.

The plant needs to pay the utility R253.13 per day under option A. However, the plant would not pay any money to the utility under option B. As for option C, the plant does not pay any money; it instead makes an income of R1452.43.

Cost analysis

The life cycle cost (LCC) and payback period (PBP) of investing in an asset are the most commonly used values in determining the attractiveness and economic viability of an investment (Ma et al. 2014; Zhang et al. 2014). The LCC is the discounted cumulative cost of owning, operating and disposing an asset. Thus,

$$\mathrm{LCC}(M) = CC + \sum_{j=0}^{M-1} \frac{OPC_j}{(1+d)^j} - DSC, \quad (12)$$

where CC, OPC_j, DSC, d and M are the capital cost, operating cash-flows at the end of the j^{th} year, disposal cost, discount rate and the useful lifetime of the asset in years, respectively. PBP is the time required for the benefits from the assets to equal the expenditure incurred to own and operate the plant. That is, the number of years that make (12) equal zero. If n_{neg} is the first year that makes the LCC negative (i.e. $\mathrm{LCC}(n_{\mathrm{neg}}) < 0$), then according to the graphical method PBP is calculated by,

$$\mathrm{PBP} = n_{\mathrm{neg}} + \frac{\mathrm{LCC}(n_{\mathrm{neg}})}{\mathrm{LCC}(n_{\mathrm{neg}}-1) - \mathrm{LCC}(n_{\mathrm{neg}})} \quad (13)$$

The OPC_j is primarily the operating income/expenses because the power electronics components under consideration are hardly ever maintained. In contrast, the motor is maintained at least twice a year (Ferreira et al. 2011). Motor cost are not included in the current case study because the plant already has suitable AC motors, and the energy saving interventions are restricted to electronic components running the motors. The electricity prices are subject to annual percentage increases r, mainly due to inflations. Thus, $\mathrm{OPC}_j = \mathrm{OPC}_0(1+r)^j$. The value of r is 13 % in accordance with the latest multi-year price determination plan by the South African regulator.[3] The electronic components of the VSD, AFE and BU are long-lasting; however, they are more likely to be replaced at the end of the lifetime of the motors that they were connected to, mainly due to technological changes. Therefore, the residual value of the electronic components is taken to be zero, i.e $\mathrm{DSC} = 0$. For the same reason, a 15-year lifetime period, M, commonly used for induction motors above 11 kW, is adopted (Ferreira et al. 2011). The methodology of calculating d for energy projects is an active area of research as recently argued in Andor and Dűlk (2015). This topic is beyond the scope of the current paper. For simplicity, the discount rate value of 2.45 % is adopted as suggest by Ferreira et al. (2011).

For the purpose of the current analysis, the investment into a cooling system for the braking resistor is deemed unnecessary. A suitable distribution transformer that connects the plant to the utility is assumed to be available at no extra cost. The salvage value of the electronic equipment is ignored. Table 2 shows the equipment cost based on technologies similar to Altivar.[4] An installation cost of 10 % of the cost of equipment is added to the CC for both options A and B. However, 20 % is added for option C because it involves an AFE, which is a rarely used component.

Table 3 shows the economic data calculations for each option and the base case. The CC calculations are obtained by summing the cost of required components from Table 2 and adding the installation costs. Table 3 shows that options A and B consume less energy from the grid than the base case, while option C feeds energy back into the grid. Option A calculations show that simply installing VSDs and implementing VSC gives an attractive PBP of 3.56 years. A comparison of options A and B shows that improving energy efficiency by using the internally generated energy becomes a better investment option with a PBP of 2.88 years. The use of a RD in option C gives the quickest PBP of 1.62 years even thought the investment costs are almost twice that of the base case.

[3] www.nersa.org.za (Multi-year price determination 2 of 2015/16)

[4] http://www.schneider-electric.com/

Table 2 Equipment prices and cost estimates

Item	Amount
	(R ≈ 0.09 US dollars as at 1 Jan 2015)
VSD 75 kW	114,695.00
VSD 315 kW	394,352.00
Active front end	278,538.00
Braking unit (chopper and resistor)	64,367.00
Accessories (DC-bus)	65,590.00

Sensitivity analysis

Discount rate and electricity price increase rate

The anticipated annual increase in electricity prices is based on the most recent increase. The calculations in Table 3 assume that the increase is maintained in the subsequent years. However, this may not be case since it depends on future market dynamics. The discount rate values are also tricky to determine because they account for time value of money from the CBS operator perspective. Some analyses estimate it using the weighted average cost of capital (WACC) of the investing entity while others base it on the difference between interest rate and inflation (Ferreira et al. 2011; Ondraczek et al. 2015). For this reason, there is an inherent uncertainty in values of both r and d. Therefore, a sensitivity analysis becomes necessary in order to validate the attractiveness of the investment options under consideration.

Figure 8 shows the influence the value of r and d has on the PBP of all the three options. r and d are varied in the ranges [2,10] and [0,15], respectively. Generally, the changes in PBP are small, with the worst change being less than 10 months. This is a good indication showing that investing in any of the given energy saving options remains attractive in spite of the likely changes in both r and d. The results show that option C is the least affected by the changes, while option A is mostly affected. The long PBP of A makes it the most vulnerable to the changes. This means that investing in RDs (option C) is a better option than A or B when the required investment cash is available. Figure 8 also shows that changes in r have a bigger impact on PBP than changes in d. For example, a 7 % change in r results in about 5 months of change in PBP while a 7 % change in d gives less than a 3 months worth of change in PBP, for option A.

Intermediate storage capacity

The intermediate bulk storage, ST1, is a typically small storage located at a transfer station to facilitate

Table 3 Benefit analysis of the different configuration options

Item	Configuration option			
	Base case	A	B	C
CC (R)	504,591.00	630,755.00	685,755.00	949,768.00
Daily energy use from utility (kWh)	923	437	0	-1984
Daily (cost) or savings (R)	(895.62)	642.49	895.62	895.62
Daily energy incomes (R)	–	–	–	1,452.43
OPC_0(R)	214,949.00	-154,198.00	-214,949.00	-563,532.00
PBP (years)	–	3.56	2.88	1.62

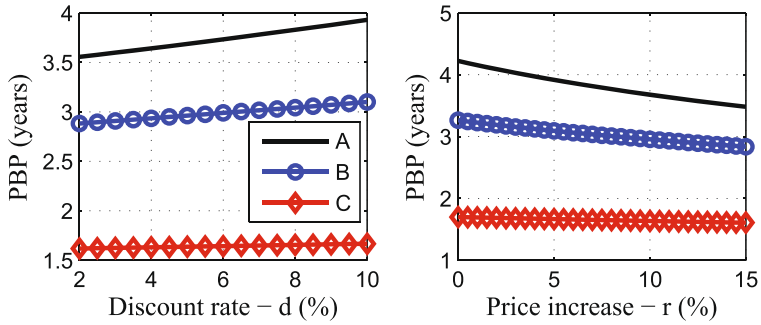

Fig. 8 Sensitivity to discount rate and electricity price increases

the exchange of material between the two belts. The use of transfer stations is usually discouraged in CBSs designs because they result in the loss of speed of material being transported and so reducing the efficiency. However, implementing a transfer station with a larger storage capacity introduces flexibility into the system and allows the system to take advantage of a time-of-use (TOU) tariff. Improved storage and feeder designs can also be applied to alleviate the problem of efficiency losses (Roberts 2003).

Figure 9 shows option C's PBP for different sizes of ST1 relative to the current size of ST2 (1680 t). Results in Fig. 9 show that increasing the storage size reduces PBP, since the daily incomes generally increase with storage size . However, increasing ST1 beyond 1680 t (or 100 %) results in a diminishing decrease in PBP until no further change happens. This is because the daily schedule cannot be optimised further to benefit from the tariff, within the given operational constraints. Therefore, an analysis similar to this required before a embarking on changing intermediate storage sizes with the aim of benefiting from the electricity tariff.

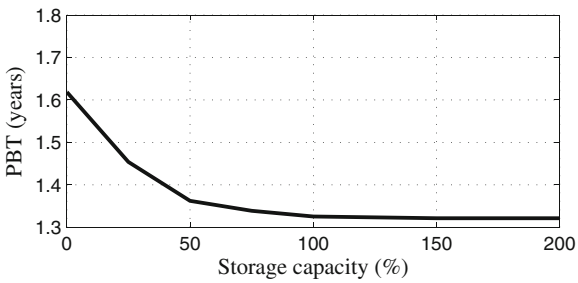

Fig. 9 Sensitivity to changes in the intermediate capacity storage, ST1

Conclusion

A generic optimal scheduling model for deriving energy-efficient and cost-effective schedules for conveyor belts systems (CBSs) with downhill belts is proposed and applied. The proposed optimisation model is able to control a CBS in order to save energy and cost within a TOU tariff that allows reselling of electricity to the grid. The model is applied on the three proposed configurations to be retro-fitted on an existing plant. These configurations use variable speed and regenerative drives. The results shows that the energy efficiency of CBS can be improved using variable speed drives (VSDs) and regenerative drives (RDs).

An economic analysis of investing in the three proposed retro-fit configurations is carried-out, based on the payback period (PBP). The PBP's sensitivity to CBS storage sizes, increase in discount rate and electricity prices is assessed. The payback periods for all the three energy-saving configurations are found to be less than 5 years over a varying range of discount rate and electricity increases. Increasing the size of CBS storages is shown to provide a limited benefit towards cost saving on the given TOU tariff. The sensitivity analysis indicates that a careful study of the effect of storage size must be carried out because increasing storage capacity results in economic gains that are generally not proportional to the size of increase.

A similar generic optimisation model and economic analysis can be performed for other similar motor-driven applications capable ofimplementing RDs. These applications includes lifts and cranes where the loads lifted above ground level present a potential source of energy. In these applications,

controlled lowering of a heavy load generates energy. In a similar manner, the counter weight of the lift can generate energy when an empty or lightly loaded lift is raised.

Appendix: Discrete version of the transport equation

The flow model Eq. 1 is discretised into N_x samples in space and N_t samples in time over a given total time period using a finite difference method . The implicit backward finite difference method is chosen due to its stability (Trefethen 1996). Therefore, Eq. 1 becomes,

$$\frac{q(i,n+1)-q(i,n)}{\Delta t} + v_n \frac{q(i+1,n+1)-q(i-1,n+1)}{2\Delta x} = 0. \quad (14)$$

A backward space derivative difference is used for the tail end of the conveyor because $q(N_x+1,n)$ is invalid. Let, $\gamma_n = v_n \frac{\Delta t}{\Delta x}$, then the algebraic manipulation of the Eq. 14 results into,

$$q(i,n+1) = \begin{cases} 2\{q(i-1,n)-q(i-1,n+1)\}/\gamma_i + q(i-2,n+1) & i = 2,3,\ldots N_x-1 \\ \{q(N_x,n)-q(N_x-1,n+1)\}/(\gamma_i+1) & i = N_x \end{cases}. \quad (15)$$

Equation 15 can be also be written in matrix and vector form as,

$$\widehat{A}_n \mathbf{q}_{n+1} = \{\mathbf{q}_n + \bar{\mathbf{b}}_n \cdot I_n / v_n\} \text{ where } \widehat{A}_n \in \mathcal{R}^{N_x \times N_x}, \bar{\mathbf{b}}_n \in \mathcal{R}^{N_x \times 1}, \quad (16)$$

where $\mathbf{q}_n$ is a vector $q(i,n)\ \forall\ i \in [1, N_x]$ and, the matrices $\widehat{A}_n$ and vectors $\bar{\mathbf{b}}_n$ are defined by,

$$\widehat{A}_n = \begin{bmatrix} 1 & \gamma_n/2 & 0 & \cdots & 0 & 0 & 0 \\ -\gamma_n/2 & 1 & -\gamma_n/2 & & 0 & 0 & 0 \\ 0 & -\gamma_n/2 & 1 & \ddots & 0 & 0 & 0 \\ \vdots & & \ddots & \ddots & \vdots & \vdots & \vdots \\ 0 & 0 & 0 & & 0 & 0 & 0 \\ 0 & 0 & 0 & & -\gamma_n/2 & 1 & \gamma_n/2 \\ 0 & 0 & 0 & & 0 & -\gamma_n & (1+\gamma_n) \end{bmatrix} \text{ and } \bar{\mathbf{b}}_n = \begin{bmatrix} \gamma_n/2 \\ 0 \\ 0 \\ 0 \\ \vdots \\ 0 \\ 0 \end{bmatrix}. \quad (17)$$

References

ABB (2011). Technical guide no. 8—electrical braking. (online). http://www.abb.com.

ABB (2011). Technical guide no. 1—direct torque control—the world's most advanced AC drive technology. (online). http://:www.abb.com.

de Almeida, A.T., Ferreira, F.J.T.E., & Both, D. (2005). Technical and economical considerations in the application of variable-speed drives with electric motor systems. *IEEE Trans. Ind Appl.*, *41*(1), 188–99.

Andor, G., & Dűlk, M. (2015). Cost of capital estimation for energy efficiency project through a cash flow beta approach. *Energy efficiency*, *8*, 365–84. doi:10.1007/s12053-014-9298-y.

Bose, B.K. (2002). Modern power electronic and AC drives, 10-11, Prentice Hall, Inc., Upper Saddle River, New Jeysey, USA.

CEMA. (2005). *Belt conveyor for bulk material*, 6th edn. Florida: Conveyor Equipment Manufacturers Association, Naples.

Eskom (2013a). Eskom submittion to nersa for Genflex tariff and incoporation of the MEC into the NMD rules. http://www.eskom.co.za.

Eskom (2013b). Tariff and charges booklet 2013/14. http://www.eskom.co.za.

Fedorko, G., Molnar, V., Marasova, D., Grincova, A., Dovica, M., Zivcak, J., Toth, T., & Husakova, N. (2014). Failure analysis of belt conveyor damage caused by the falling material. Part I: experimental measurements and regression models. *Eng Fail Anal*, *36*, 30–8. doi:10.1016/j.engfailanal.2013.09.017.

Ferreira, F.J.T.E., Fong, J.A.C., & de Almeida, A.T. (2011). Ecoanalysis of variable-speed drives for flow regulation in pumping systems. *IEEE Trans Ind Electron*, *58*(6), 2117–25. doi:10.1109/TIE.2010.2057232.

Gellings, C.W., & Samotyj, M. (2013). Smart grid as advanced technology enabler of demand response. *Energy efficiency*, *6*, 685–94. doi:10.1007/s12053-013-9203-0.

González-Gil, A., Palacin, R., & Batty, P. (2013). Sustainable urban rail systems: strategies and technologies for optimal management of regenerative braking energy. *Energ Convers Manage*, *75*, 374–88. doi:10.1016/j.enconman.2013.06.039.

Hiltermann, J., Lodewijks, G., Schott, D.L., Rijsenbrij, J.C., Dekkers, J.A.J.M., & Pang, Y. (2011). A methodology to predict power saving of troughed belt conveyors by speed control. *Particul Sci Technol*, *29*(1), 14–27. doi:10.1080/02726351.2010.491105.

Kouro, S., Rodríguez, J., Wu, B., Bernet, S., & Perez, M. (2012). Powering the future of industry—high power adjustable speed drive topologies. *IEEE Ind. Appl. Mag.*, *18*(4), 26–39.

ISO (1989). Continuous mechanical handling equipment—belt conveyor with carrying idlers—calculation of operating power and tensile forces. *ISO*, 5048.

Lűchinger, P., Maier, U., & Errath, R.A. (2006). Active front end technology in the application of a down hill conveyor. In *Cement Industry Technical Conference, 2006. Conference Record. IEEE*. doi:10.1109/CITCON.2006.1635717.

Ma, T., Yang, H., & Lu, L. (2014). Feasibility study and economic analysis of pumped hydro storage and battery storage for a renewable energy powered island. *Energy Convers and Manage*, *79*, 387–97. doi:10.1016/j.enconman.2013.12.047.

Madlool, N., Saidur, R., Rahim, N., & Kamalisarvestani, M. (2013). An overview of energy savings measures for cement industries. *Renew Sust Energ Rev*, *19*, 18–29. doi:10.1016/j.rser.2012.10.046.

Mathaba, T., Xia, X., & Zhang, J. (2012). Optimal scheduling of conveyor belt systems under critical peak pricing. In *International Power and Energy Conference (IPEC), 2012, Ho Chi Minh City, Vietnam, pp. 315–20*.

Mathaba, T., Xia, X., & Zhang, J. (2014). Analysing the economic benefit of electricity price forecast in industrial load scheduling. *Electr Pow Syst Res*, *116*(0), 158–65. doi:10.1016/j.epsr.2014.05.008.

Middelberg, A., Zhang, J., & Xia, X. (2009). An optimal control model for load shifting—with application in the energy management of a colliery. *Appl Energ*, *86*(7-8), 1266–73.

Mitrovic, N., Petronijevic, M., Kostic, V., & Jeftenic, B. (2012). Electrical drives for crane application. InTech, Rijeka, Croatia. http://www.intechopen.com/books/mechanical-engineering/electrical-drives-for-crane-application.

Musolino, V., Pievatolo, A., & Tironi, E. (2011). A statistical approach to electrical storage sizing with application to the recovery of braking energy. *Energy*, *36*(11), 6697–704. doi:10.1016/j.energy.2011.07.037.

Ondraczek, J., Komendantova, N., & Patt, A. (2015). WACC the dog: the effect of financing costs on the levelized cost of solar PV power. *Renew Energ*, *75*, 888–98. doi:10.1016/j.renene.2014.10.053.

Pelzer, R., Mathews, E., le Roux, D., & Kleingeld, M. (2008). A new approach to ensure successful implementation of sustainable demand side management (DSM) in South African mines. *Energy*, *33*(8), 1254–63. doi:10.1016/j.energy.2008.03.004.

Ristić, L. B., & Jeftenić, B. I. (2012). Implementation of fuzzy control to improve energy efficiency of variable speed bulk material transportation. *IEEE Trans Ind Electron*, *59*(7), 2959–68.

Roberts, A. (2003). Chute performance and design for rapid flow conditions. *Chem Eng Technol*, *26*(2), 163–70. doi:10.1002/ceat.200390024.

Rodríguez, J., Pontt, J., Alzamora, G., Becker, N., Einenkel, O., & Weinstein, A. (2002). Novel 20-MW downhill conveyor system using three-level converters. *IEEE Trans Ind Electron*, *49*, 1093–100.

Rodríguez, J., Jih-Sheng, L., & Fang, Z. P. (2002). Multilevel inverters: a survey of topologies, control and applications. *IEEE Trans Ind Electron*, *49*(4), 724–738.

Saidur, R., Mekhilef, S., Ali, M., Safari, A., & Mohammed, H. (2012). Applications of variable speed drive (VSD) in electrical motors energy savings. *Renew Sust Energ Rev*, *16*(1), 543–50. doi:10.1016/j.rser.2011.08.020.

Schneider-Electric (2013). Active front end—options for Altivar 61 and Altivar 71. (online). http://www.schneider-electric.com/.

Strauss, W.A. (2008). Partial differential equations—an introduction, 2nd edn. 10–11, John Wiley & Sons, Inc., Hoboken, New Jeysey, USA.

Trefethen, L.N. (1996). *Finite difference and spectral methods for ordinary and partial differential equations*: Cornell University.

vanDelft, T. J. (2010). Modeling and model predictive control of a conveyor-belt dryer—applied to the drying of fish feed. Master's thesis, Norwegian University of Science and Technology.

Zhang, J., Lv, C., Qiu, M., Li, Y., & Sun, D. (2013). Braking energy regeneration control of a fuel cell hybrid electric bus. *Energ Convers Manage*, *76*, 1117–24. doi:10.1016/j.enconman.2013.09.003.

Zhang, L., Xia, X., & Zhang, J. (2014). Improving energy efficiency of cyclone circuits in coal beneficiation plants by pump-storage systems. *Appl Energ*, *119*(0), 306–13. doi:10.1016/j.apenergy.2014.01.031.

Zhang, S., & Xia, X. (2010). Optimal control of operation efficiency of belt conveyor systems. *Appl Energ*, *87*, 1929–37.

Zhang, S., & Xia, X. (2011). Modeling and energy efficiency optimization of belt conveyors. *Appl Energ*, *88*(9), 3061–71.